PNAS RESEARCH ARTICLE | BIOCHEMISTRY

Scribble scrambles parathyroid hormone receptor interactions to regulate phosphate and vitamin D homeostasis

Bryce Z. Stewart[a], Tatyana Mamonova[b], W. Bruce Sneddon[b], Airah Javorsky[a], Yanmei Yang[b,1], Bin Wang[b,1], Thomas D. Nolin[c,d], Patrick O. Humbert[a,e,f], Peter A. Friedman[b,2], and Marc Kvansakul[a,2]

Edited by Robert Lefkowitz, Howard Hughes Medical Institute, Durham, NC; received December 7, 2022; accepted March 30, 2023

G protein-coupled receptors, including PTHR, are pivotal for controlling metabolic processes ranging from serum phosphate and vitamin D levels to glucose uptake, and cytoplasmic interactors may modulate their signaling, trafficking, and function. We now show that direct interaction with Scribble, a cell polarity-regulating adaptor protein, modulates PTHR activity. Scribble is a crucial regulator for establishing and developing tissue architecture, and its dysregulation is involved in various disease conditions, including tumor expansion and viral infections. Scribble co-localizes with PTHR at basal and lateral surfaces in polarized cells. Using X-ray crystallography, we show that colocalization is mediated by engaging a short sequence motif at the PTHR C-terminus using Scribble PDZ1 and PDZ3 domain, with binding affinities of 31.7 and 13.4 μM, respectively. Since PTHR controls metabolic functions by actions on renal proximal tubules, we engineered mice to selectively knockout Scribble in proximal tubules. The loss of Scribble impacted serum phosphate and vitamin D levels and caused significant plasma phosphate elevation and increased aggregate vitamin D_3 levels, whereas blood glucose levels remained unchanged. Collectively these results identify Scribble as a vital regulator of PTHR-mediated signaling and function. Our findings reveal an unexpected link between renal metabolism and cell polarity signaling.

cell polarity | GPCR | PTHR | Scribble | phosphate homeostasis

Significance

G protein-coupled receptors such as PTHR critically control metabolic processes, including serum phosphate and vitamin D levels. We now show that direct interaction with Scribble, a cell polarity-regulating adaptor protein, controls PTHR activity. Scribble engages a short sequence motif at the PTHR C-terminus using its PDZ1 and PDZ3 domain to bind with micromolar affinities. The loss of this interaction impacts serum phosphate and vitamin D levels in Scribble KO mice. Our findings reveal an unexpected link between renal metabolism and cell polarity signaling.

Cell polarity is a key feature of eukaryotic cells and fulfills a critical role in tissue development and the correct establishment of tissue architecture (1). Within a cell, cell polarity leads to the asymmetric distribution of macromolecules, including proteins, lipids, and carbohydrates, into distinct cellular domains. This phenomenon gives rise to apical-basal cell polarity (2). Apical–basal cell polarity is critical for regulating crucial cellular signaling pathways, including apoptosis, vesicle trafficking, cell proliferation, and migration (3). Notably, the loss of cell polarity is a defining hallmark of cancer development. At the molecular level, the dynamic interplay between three key polarity modules, Scribble, Par, and Crumbs, mediates apical-basal cell polarity (4). Scribble is a master regulator of cell polarity and, together with Discs-large (Dlg), and Lethal-Giant-Larvae (Lgl), forms the Scribble polarity module. Initially discovered in *Drosophila melanogaster* as a tumor suppressor (5), Scribble plays an essential role in tumor initiation. Combined with oncogenic drivers, including RAS, Scribble loss can drive tumor progression in multiple epithelial tissue types such as mammary, prostate, skin, and lung (6). Furthermore, Scribble also regulates polarity and signaling in many cell types and organisms, playing a crucial role in organ development and physiology (7).

Scribble is composed of 16 Leucine-Rich Repeats, 2 LAP-Specific domains and 4 PSD-95/Disc-large/ZO-1 (PDZ) domains and is a member of the LAP family of proteins (6). As a signaling adaptor protein, the vast majority of Scribble interactions are mediated via its PDZ domains, thus enabling Scribble to act on multiple discrete signaling pathways (3). Short amino acid sequences often found at the very C-termini of interacting proteins, referred to as PDZ-binding motifs (PBMs), mediate interactions of Scribble PDZ domains. PBMs are divided into three classes, with class 1 PBMs consisting of X-T/S-X-Φ_{COOH} (where X is any residue and Φ is any hydrophobic residue), class 2 being X-Φ-X-Φ_{COOH} and class 3 is X-D/E-X-Φ_{COOH} (8–10).

The parathyroid hormone receptor (PTHR) is the canonical G protein-coupled receptor (GPCR) for PTH and PTHrP. It regulates phosphate homeostasis and serum 1,25$[OH]_2$-vitamin D (1,25$[OH]_2$D) levels by actions on proximal renal tubules. Most GPCRs are found at apical or basolateral cell membranes (11), and PTHR is expressed at the apical and basolateral membranes of proximal tubule cells (12–14). At apical cell membranes, PTHR binds NHERF1, a PDZ scaffold protein that regulates G protein signaling and is required for hormone-sensitive apical phosphate uptake by the NPT2A

Author contributions: B.Z.S., T.M., P.O.H., P.A.F., and M.K. designed research; B.Z.S., T.M., W.B.S., A.J., Y.Y., B.W., T.D.N., and M.K. performed research; B.Z.S., T.M., W.B.S., A.J., Y.Y., B.W., T.D.N., P.O.H., P.A.F., and M.K. analyzed data; and B.Z.S., T.M., P.O.H., P.A.F., and M.K. wrote the paper.

The authors declare no competing interest.

This article is a PNAS Direct Submission.

[1]Present address: Center for Translational Medicine, Departments of Medicine, Sidney Kimmel Medical College, Thomas Jefferson University, Philadelphia, PA 19107.

[2]To whom correspondence may be addressed. Email: paf10@pitt.edu or m.kvansakul@latrobe.edu.au.

This article contains supporting information online at https://www.pnas.org/lookup/suppl/doi:10.1073/pnas.2220851120/-/DCSupplemental.

Published May 30, 2023.

Na-phosphate transporter (15, 16). Differential PTHR signaling of apical and basolateral PTHR has been reported (12, 17), but the functional consequences of this asymmetry are unknown, as are the mechanisms underlying bilateral receptor localization. While characterizing interactions of PTHR with NHERF1, we unexpectedly discovered that NHERF1 downregulation relocates PTHR to basolateral membranes. This observation raised the question of whether an analogous basolateral PDZ protein might tether PTHR at basolateral cell surfaces. The basolateral GPCR localization has generally been ascribed to the presence of encoded sorting motifs (YXXΦ and LL) and targeted phosphorylation upon the formation of cell-cell junctions (18, 19). Remarkably few basolateral PDZ proteins have been described. Scribble, a multi-PDZ domain protein involved in morphogenesis and cell polarity (20) is found at basolateral cell surfaces (21), raising the possibility that Scribble is a putative PTHR molecular partner. However, no interaction has been described previously. Here we report the molecular and functional characterization of the interaction of Scribble with PTHR. Our findings reveal a previously undiscovered link between polarity signaling and hormone receptor signaling.

Results

PTHR Colocalizes with Scribble in MDCK Cells. Scribble directly interacts with a diverse repertoire of cellular interactors to modulate signaling, including the Guanine Nucleotide Exchange Factor β-PIX and the membrane protein Vangl2 (22,

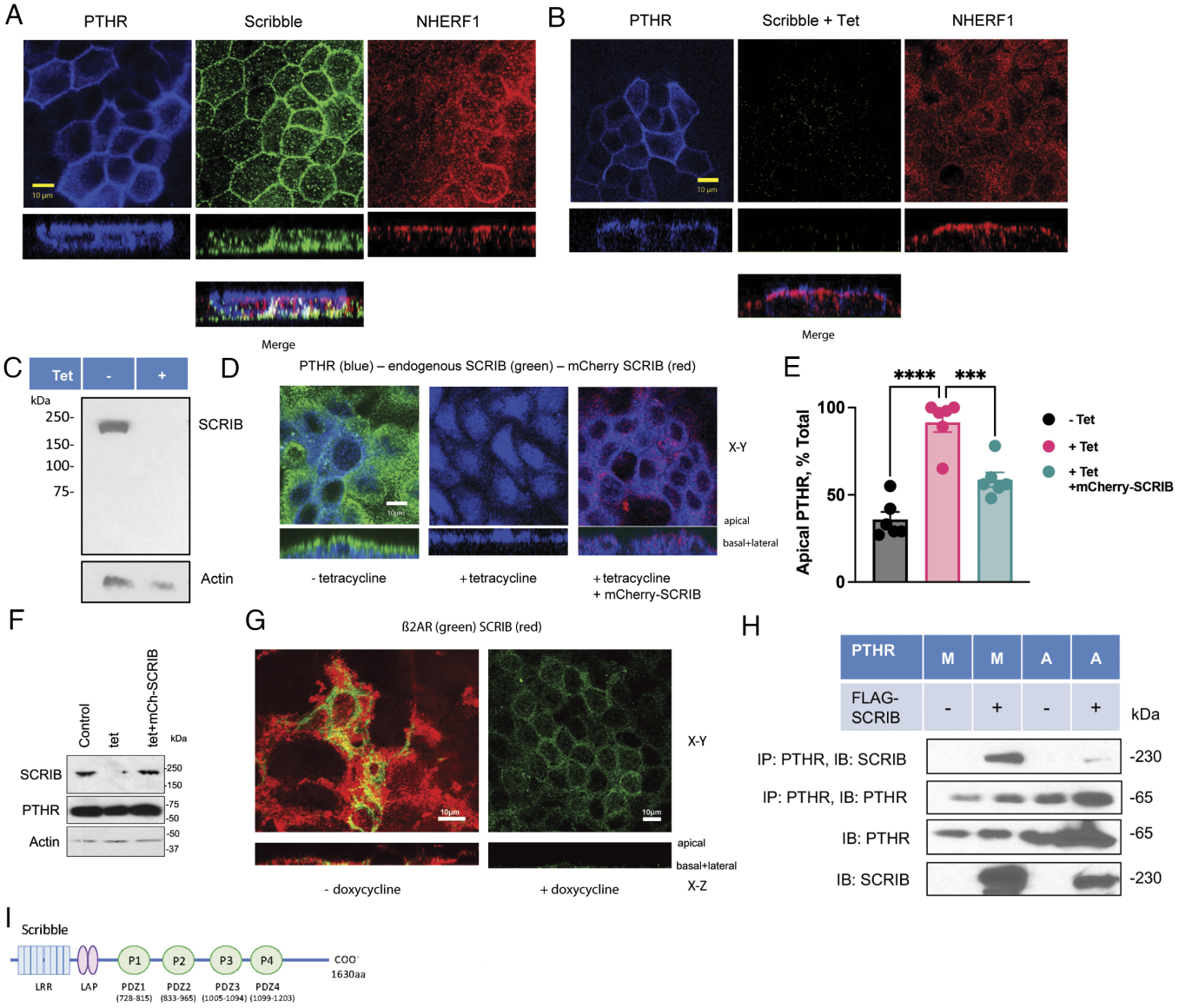

Fig. 1. Interactions of PTHR and Scribble. PTHR (blue) interacts with Scribble (Scrib, green), and NHERF1 (red) under control conditions (*A*) in MDCK cells stably expressing PTHR and Scribble shRNA in a tetracycline-inducible manner (MDCK-pTR Scribble shRNA. Following 10 μg/mL^{-1}/16 h tetracycline (Tet) treatment (*B*), PTHR is associated only with NHERF1 at apical cell membranes. X-Y planes are shown in the *Upper* panels, and the corresponding X-Z plane below. (*C*) Western blot of Scrib knockdown in MDCK cells using Scribble shRNA. (*D*) Rescue of SCRIB knockdown redistributes the PTHR to basal and lateral membranes. PTHR-MDCK-shSCRIB cells were treated with 10 mg/mL tetracycline (tet) overnight followed by transfection with HA-mCherry-SCRIB, as indicated. SCRIB (green), PTHR (blue), and rescued SCRIB (red) are depicted (*E*) Apical PTHR expression was quantified as % Total using Image J for replicate experiments identical to those depicted in 1D. ****P < 0.0001, n = 6. (*F*). Lysates were prepared and immunoblotted for SCRIB (*Top*), PTHR (*Middle*), and actin (*Bottom*). The 10% gel doesn't permit discriminating between 225 kDa (native Scribble) and 248 kDa (HA-mCherry-SCRIB). (*G*) SCRIB (red) knockdown failed to disrupt basolateral ADRB2 (green). (*H*) Immunoprecipitation of PTHR with Scribble in HEK293 cells. (*I*) Domain organization of Scribble. PDZ domain boundaries correspond to those used for purified recombinant PDZ domains.

23). However, no interaction with PTHR has previously been reported. Consequently, we first sought to establish whether PTHR colocalizes with Scribble in intact cells. In fixed Madin-Darby Canine Kidney (MDCK) cells stably expressing HA-tagged PTHR, NHERF1 (red) primarily localized to the apical surface, whereas Scribble (green) was expressed at basal and lateral surfaces (Fig. 1*A*). PTHR, shown in blue, is distributed to both apical and basolateral membranes, as depicted in the orthogonal view. Upon tetracycline-induced (Tet) SCRIB knockdown, PTHR virtually disappeared from basolateral surfaces but remained associated with NHERF1 at apical plasma membranes (Fig. 1 *B*–*D*). The shift of PTHR localization from basolateral to apical surfaces after the loss of Scribble could be rescued by re-expressing mCherry-tagged Scribble (Fig. 1 *D* and *E*). By the virtue of its size, mCherry-SCRIB (250 kDa) is challenging to transfect, and expression is lower than endogenous SCRIB in control cells (-tetracycline). Nonetheless, sufficient mCherry-SCRIB is present to rescue and redistribute PTHR, as shown. mCherry-SCRIB migrates at a marginally

A

PTHR peptide sequence	Interaction	N	K_D (μM)	ΔH (kcal·mol-1)	-TΔS (kcal·mol-1·K-1)	ΔG
ETVM	PDZ1:PTHR 4mer	1.1 ± 0.15	56.98 ± 0.23	-1.00 ± 0.01	-4.79 ± 0.02	-5.79 ± 0.01
QEEWETVM	PDZ1:PTHR 8mer	1.15 ± 0.15	31.72 ± 4.47	-0.69 ± 0.33	-5.45 ± 0.28	-6.14 ± 0.06
DEEASGPERPP ALLQEEWETVM	PDZ1:PTHR 22mer	1.1 ± 0.04	11.53 ± 1.7	-0.49 ± 0.07	-6.23 ± 0.02	-6.73 ± 0.05
	PDZ2:PTHR 4mer	NB	NB	NB	NB	NB
	PDZ2:PTHR 8mer	NB	NB	NB	NB	NB
	PDZ2:PTHR 22mer	NB	NB	NB	NB	NB
	PDZ3:PTHR 4mer	1.1 ± 0.03	17.11 ± 4.17	-3.76 ± 0.26	-2.75 ± 0.40	-6.53 ± 0.14
	PDZ3:PTHR 8mer	1.0 ± 0.04	13.4 ± 0.94	-2.81 ± 0.35	-3.84 ± 0.38	-6.65 ± 0.03
	PDZ3:PTHR 22mer	1.05 ± 0.11	11.53 ± 1.7	-8.43 ± 1.12	1.99 ± 1.11	-6.44 ± 0.01
	PDZ4:PTHR 4mer	NB	NB	NB	NB	NB
	PDZ4:PTHR 8mer	NB	NB	NB	NB	NB
	PDZ4:PTHR 22mer	NB	NB	NB	NB	NB

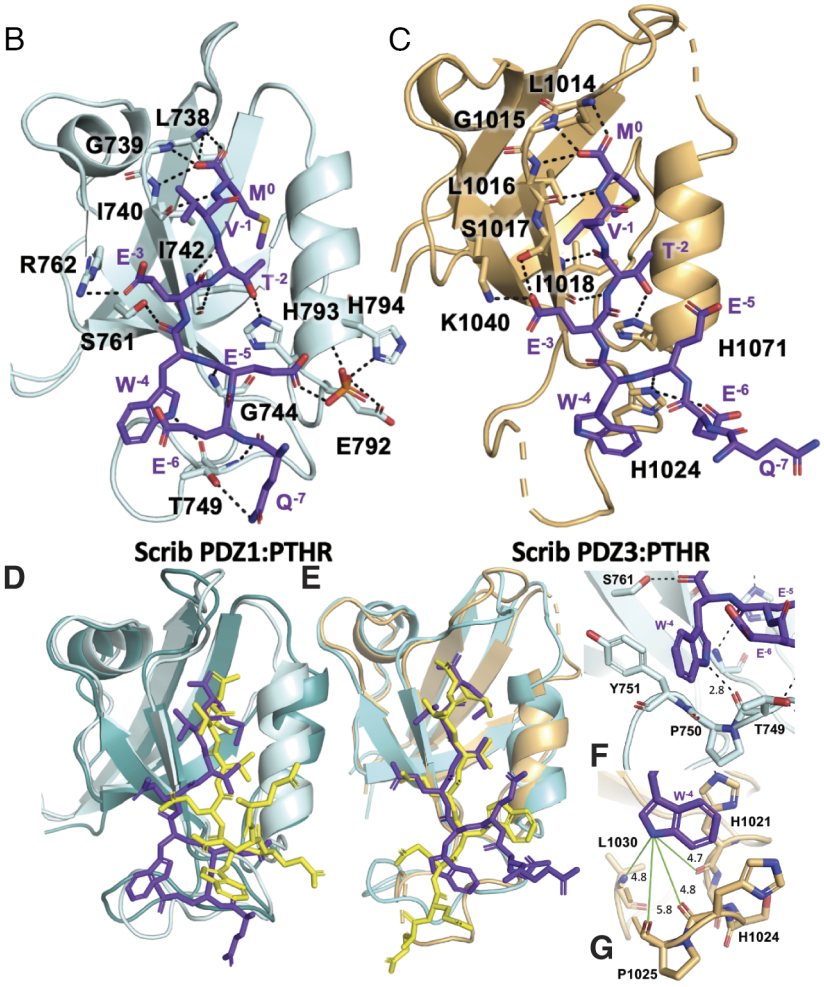

Fig. 2. Interactions of Scribble PDZ1 and PDZ3 domains with PTHR PBM. The PTHR-P 8-mer PBM peptide interacts with Scribble PDZ1 and PDZ3 via the canonical groove between β strand 2 and α helix 2. (*A*) Affinity and thermodynamic binding parameters for SCRIB PDZ domains interactions with C-terminal PBM peptides of PTHR. NB denotes no binding. Each of the values was calculated from at least three independent experiments. Each of the values was calculated from at least three independent experiments with errors as SD. (*B*) PDZ1 (pale cyan) is represented as cartoon with residues involved in interactions and the PTHR-P 8-mer peptide (purple) shown as sticks. (*C*) PDZ3 (light orange) is represented as cartoon with residues involved in interactions and the PTHR-P 8-mer peptide (purple) shown as sticks. (*D*) Scribble PDZ1:PTHR complex vs simulated MD model (deep teal:yellow) orientations of PTHR PBM. (*E*) Scribble PDZ3:PTHR complex vs simulated MD model (deep teal:yellow) orientations of PTHR PBM. (*F*) Position of PTHR W^{-4} in PDZ1 binding groove. Hydrogen bonds are indicated by black dashed lines. (*G*) Position of PTHR W^{-4} in PDZ3 binding groove. The distances of the indole ring nitrogen to putative hydrogen bonding partners are shown as solid green lines with distances given in Å and marked in black, revealing that the nitrogen is too distant from the β2/3 loop to form hydrogen bonds.

greater size than native Scribble (Fig. 1*F*). This apparent disparity may result partly from the relatively small (10%) difference in mass between constitutive Scribble and the fusion protein and limited gel resolution. Additionally, the cleavage of mCherry can occur during physiological degradation or turnover of Scribble or within the engineered protein-mCherry linker. The employed antibody may only detect the fraction of Scribble, where the mCherry tag has degraded. ß$_2$-adrenergic receptors (ADRB2) are ubiquitously expressed on cell membranes, including MDCK cells (24). SCRIB knockdown failed to disrupt basolateral ADRB2 (Fig. 1*G*). To confirm a direct interaction between PTHR and Scribble, we next performed immunoprecipitation experiments using HEK 293 cells, where overexpressed PTHR and Scribble co-immunoprecipitated as shown by western blot (Fig. 1*G*).

Isolated Scribble PDZ Domains Specifically Interact with the PHTR PBM. To further understand the putative interaction(s) of PTHR with Scribble, we examined the affinity of recombinant isolated Scribble PDZ1, 2, 3, and 4 domains (Fig. 1*H*) for three peptides corresponding to the class I PBM located at the cytoplasmic tail of PTHR. Our ITC measurements revealed that an 8-mer PTHR PBM peptide bound to Scribble PDZ1 and PDZ3 domains with affinities of 31.7 and 13.4 μM, with no binding observed to PDZ2 and PDZ4 domains. The corresponding 22-mer PBM peptide has comparable affinities (11.5 and 19.2 μM), whereas the 4-mer peptide has 57 and 17.1 μM affinities (Fig. 2*A* and *SI Appendix*, Fig. S1).

Analysis of the thermodynamic binding parameters of PTHR PBM peptide engagement of Scribble PDZ1 and PDZ3 domains revealed the interaction of Scribble PDZ3 with the 22-mer PTHR PBM as the sole interaction to feature an unfavorable entropic contribution. In contrast, both favorable enthalpy and entropy drove all remaining interactions. Notably, all PDZ1 interactions were dominated by -TΔS, with smaller enthalpic contributions.

To examine the structural basis of PTHR PBM engagement of Scribble PDZ domains, we determined the crystal structures of Scribble PDZ1 and PDZ3 in complex with PTHR PBM (Fig. 2 *B* and *C*, *SI Appendix*, Fig. S2, and Table 1). SCRIB PDZ1:PTHR was refined to a resolution of 2.4 Å with an R_{work}/R_{free} of 0.250/0.269. PDZ1 adopts the globular PDZ fold β-sandwich structure comprised of six β-strands and two α-helices that have been previously described (23). Clear and continuous electron density is observed for PTHR PBM (*SI Appendix*, Fig. S2), which lodges in the canonical binding groove of Scribble PDZ1 formed by the β2 strand and helix α2. SCRIBBLE PDZ1 binding to PTHR PBM is achieved via the docking of $M^{0\text{-PTHR}}$ in a pocket formed by PDZ1 L^{738}, G^{739} I^{740}, and I^{742} (Fig. 2*B*), as previously observed in other PDZ1 complexes (23, 25). A salt bridge between $R^{762\ PDZ1}$ and $E^{-3\text{-PTHR}}$ supports complex formation, with main-chain mediated hydrogen bonds between $L^{738\ PDZ1}$:$M^{0\text{-PTHR}}$, $G^{739\ PDZ1}$:$M^{0\text{-PTHR}}$, $I^{740\ PDZ1}$:$M^{0\text{-PTHR}}$, $I^{742\ PDZ1}$:$T^{-2\text{-PTHR}}$, and $G^{744\ PDZ1}$:$E^{-5\text{-PTHR}}$. The main chain of $T^{749\ PDZ1}$ contributed an additional hydrogen bond with the side chain of $W^{-4\text{-PTHR}}$, and a hydrogen bond via the side chain with the side chain of $Q^{-7\text{-PTHR}}$. The side-chain of $S^{761\ PDZ1}$ contacts the main chain $W^{-4\text{-PTHR}}$, and the hallmark interaction is located at the side-chain mediated $H^{793\ PDZ1}$:$T^{-2\text{-PTHR}}$. Unexpectedly, a phosphate ion was located at the center of an interaction network featuring $H^{749\ PDZ1}$, $E^{792\ PDZ1}$ as well as $E^{-5\text{-PTHR}}$.

SCRIB PDZ3:PTHR was refined to a resolution of 2.6 Å with an R_{work}/R_{free} of 0.277/0.285. Like Scribble PDZ1, the PDZ3 domain adopts the recognized PDZ fold. Clear and continuous electron density is observed for PTHR PBM, which is bound in the canonical binding groove (Fig. 2*C* and *SI Appendix*, Fig. S2). In PDZ3, $M^{0\text{-PTHR}}$ inserts into a pocket formed by $L^{1014\ PDZ3}$, $G^{1015\ PDZ3}$ and $L^{1016\ PDZ3}$ as reported for other Scribble PDZ3 complexes with interacting PBM sequences (22, 23). Additional interactions include salt bridges between $K^{1040\ PDZ3}$ and $E^{3\text{-PTHR}}$, $H^{1024\ PDZ3}$ and $E^{-6\text{-PTHR}}$, and a dense network of hydrogen bonds: the main chain mediated $L^{1014\ PDZ3}$:$M^{0\text{-PTHR}}$, $G^{1015\ PDZ3}$:$M^{0\text{-PTHR}}$, $L^{1016\ PDZ3}$:$M^{0\text{-PTHR}}$, $I^{1018\ PDZ3}$:$T^{-2\text{-PTHR}}$, and side chain mediated $S^{1017\ PDZ3}$:$E^{-3\text{-PTHR}}$, $H^{1071\ PDZ3}$:$T^{-2\text{-PTHR}}$, and $H^{1024\ PDZ3}$ with main chain $E^{-5\text{-PTHR}}$.

Considering the unusual Scribble PDZ1 domain contact residues for the bound phosphate group, we performed MD simulations to gain insight into the binding mode of the PTHR 8-mer peptide. Our all-atom explicit-solvent 250 ns MD simulation revealed significant conformational flexibility of the PTHR PBM N-terminus, which may stabilize the presence of the phosphate. Notably, Q^{-7}, E^{-6} and E^{-5}, and W^{-4} are not involved in stable

Table 1. Crystallographic data collection and refinement statistics

	PDZ1:PTHR-PBM	PDZ3:PTHR-PBM
Data collection		
Space group	I 4_1 2_1 2	I 4_1 2 2
No of molecules in AU	1+1	1+1
Cell dimensions		
a, *b*, *c* (Å)	53.19, 53.19, 217.06	82.50, 82.50, 59.66
α, β, γ (°)	90.00, 90.00, 90.00	90.00, 90.00, 90.00
Wavelength (Å)	0.9537	0.9537
Resolution (Å)*	51.66–2.4 (2.49–2.4)	41.25–2.6 (2.69–2.6)
R_{sym} or R_{merge}*	0.047 (0.472)	0.1314 (1.134)
$I/\sigma I$*	14.2 (2.4)	13.41 (1.11)
CC(1/2)	0.999 (0.932)	0.999 (0.921)
Completeness (%)*	99.4 (98.9)	98.96 (99.38)
Redundancy*	4.4 (4.7)	3.8 (3.9)
Wilson B-factor	56.57	68.1
Refinement		
Resolution (Å)	42.84–2.4	31.25–2.6
No. reflections	6444 (623)	3135 (310)
R_{work}/R_{free}	0.250/0.269	0.277/0.285
No. non-hydrogen atoms		
Protein	830	730
Ligand/ion	5	1
Water	35	8
B-factors		
Protein	65.32	98.45
Ligand/ion	68.8	99.27
Water	63.64	89.77
rmsd		
Bond lengths (Å)	0.002	0.006
Bond angle (°)	0.47	0.51
Ramachandran plot (%)		
Favored	98.11	93.33
Allowed	1.89	6.67
Disallowed	0	0

*Values in parenthesis are for highest resolution shell.

A

	N	K_D (μM)	ΔH (kcal·mol-1)	-TΔS (kcal·mol-1·K-1)
PDZ1:PTHR 8mer	1.15 ± 0.15	31.72 ± 4.47	-0.69 ± 0.33	-5.45 ± 0.28
PDZ1-R762A:PTHR 8mer	1.0 ± 0.1	39.9 ± 2.1	-0.90 ± 0.2	17.0 ± 0.6
PDZ1-H793A:PTHR 8mer	NB	NB	NB	NB
PDZ3:PTHR 8mer	1.0 ± 0.04	13.4 ± 0.94	-2.81 ± 0.35	-3.84 ± 0.38
PDZ3-K1040A:PTHR 8mer	0.9 ± 0.1	23.5 ± 1.6	-4.71 ± 0.29	-1.60 ± 0.29
PDZ3-H1071A:PTHR 8mer	NB	NB	NB	NB

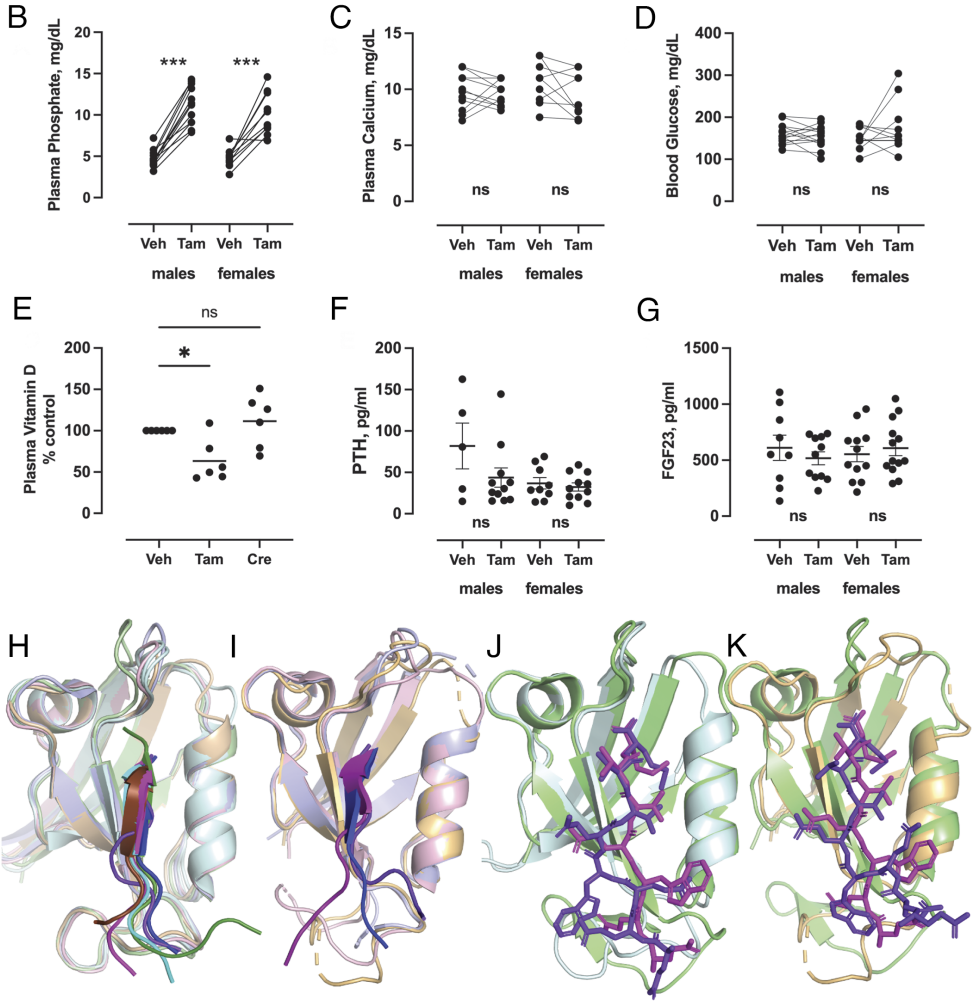

Fig. 3. Characterization of the Scribble–PTHR interaction. (*A*) Targeted mutations in PDZ1 and PDZ3 disrupt PTHR PBM binding. NB denotes no binding. Each of the values was calculated from at least three independent experiments with errors as SD. (*B*) Targeted Scribble KO mice display increased serum phosphate (*C*), normal levels of calcium and glucose (*D*), decreased 1,25$[OH]_2$-vitamin D (1,25$[OH]_2$D) levels (*E*), and normal levels of PTH and FGF23 (*F* and *G*). (*H*) Cartoon representations of the superimposition of *hs*SCRIB PDZ1:PTHR with *hs*ScribPDZ1 bound to APC (pale cyan:cyan – 6MS1), β-pix (light pink:magenta – 5VWK), MCC (wheat:chocolate – 6MTV), internal Scr Homology 3 (pale green:forest green – 6MYE) and Vangl2 (light blue:blue – 6XA8). (*I*) Cartoon representations of the superimposition of *hs*SCRIB PDZ3:PTHR with *hs*ScribPDZ3 bound to β-pix (light pink:magenta – 5VWI) and Vangl2 (light blue:blue – 6XA6). (*J*) PDZ1:PTHR superimposed with *rn*Snx27:PTHR (lime:magenta) showing different orientations of PTHR. (*K*) PDZ3:PTHR superimposed with *rn*Snx27:PTHR (lime:magenta) showing different orientations of PTHR.

interactions with PDZ1 on our MD timescale, underscoring the flexibility in this region (Fig. 2*D* and Movie S1). We also performed all-atom explicit-solvent 250 ns MD simulations to explore the binding modes of the PTHR-P 8-mer peptide bound to the PDZ3 domain. Interestingly, the simulated PDZ3 complex revealed that W^{-4} from PTHR can engage helix α2, suggesting significant conformational flexibility in how residues upstream of the four C-terminal PBM residues interact with the canonical PDZ binding groove (Fig. 2 *E*–*G* and Movie S2).

To validate our crystal structures, we performed site-directed mutagenesis and evaluated the impact of the mutations on PTHR binding to Scribble PDZ1 and PDZ3 domains. PDZ1 R762A and PDZ3 K1040A have mildly reduced affinities for PTHR PBM of 39.9 and 23.5 μM, respectively, whereas PDZ1 H793A and PDZ3 H1071A lost the ability to bind PTHR PBM (Fig. 3*A* and *SI Appendix*, Fig. S1).

Loss of Scribble Impacts Renal Phosphate Homeostasis and Serum Vitamin D Levels. Having established that PTHR and Scribble colocalize in intact cells and that peptides encoding for the PBM of PTHR directly interact with Scribble PDZ domains 1 and 3, we next sought to establish the physiological role of this interaction. For this purpose, Scribble was knocked out in proximal tubules, and the impact of targeted Scribble loss in

renal proximal tubules on phosphate homeostasis and serum 1,25$[OH]_2$-vitamin D (1,25$[OH]_2$D) levels was examined.

Tamoxifen (Tam)-induced Scribble knockout caused significant plasma phosphate elevation equivalently in male and female mice (Fig. 3*B*). Combined 1,25$(OH)_2D_3$ + 24,25$(OH)_2D_3$ + 24(OH)D_3 levels, as indicated in Methods, decreased only in Tam-injected animals and not in corresponding Cre littermates (Fig. 3*E*). To exclude non-specific renal tubular damage, we measured serum glucose levels (Fig. 3*D*), which were unchanged. Similarly, plasma calcium concentration (Fig. 3*C*), PTH (Fig. 3*F*) and FGF23 (Fig. 3*G*) levels remained unchanged.

Discussion

PTHR binds to NHERF1, a PDZ domain-containing scaffold protein (26–28). Utilizing PDZ1 and two domains via a C-terminal class I PBM, NHERF1 can modify the signaling, trafficking, and function of the GPCR PTHR. We now show that in addition to NHERF1, PTHR can also interact with Scribble with distinct colocalization observed in MDCK cells. Direct binding of the PTHR PBM with Scribble PDZ1 and PDZ3 domains mediates the interaction of PTHR with Scribble. The affinity and mode of engagement of PTHR PBM for Scribble PDZ1 and PDZ3 are comparable to other previously examined endogenous Scribble interactions such as β-PIX, APC, MCC, or Vangl2 (22, 23, 25, 29) (Fig. 3 *H* and *I*). Loss of the canonical histidine in the PDZ1 and PDZ3 binding groove ablates the interaction. However, a comparison of PTHR binding to the PDZ domain of Snx27 (Fig. 3 *J* and *K*) with SCRIB PDZ1 and PDZ3 reveals that W^{-4} PTHR PBM can engage multiple sites on both sides of the canonical PDZ binding groove, thus driving the formation of differential conformations of the N-termini of the PTHR PBM in all three complexes. This is supported by molecular dynamics analysis, which revealed that PTHR PBM residues beyond the four key interacting residues at the very C-terminus display substantial conformational flexibility, including W^{-4}. Indeed, the W^{-4} in the PTHR PBM forms hydrogen bonds via the nitrogen in the indole ring in the SCRIB PDZ1 complex (Fig. 2*F*), whereas in the SCRIB PDZ3 complex it is located too distal from potential hydrogen bond interactors in the β2/3 loop. Instead, W^{-4} side chain ring stacks with SCRIB PDZ3 H1021 (Fig. 2*G*). Whether or not additional interactions that contribute to PTHR-Scribble interactions exist beyond the PDZ domain interactions with the PBM motif remains unclear. Structural analysis of the nearly full-length PTHR using cryo-EM (30) revealed the detailed receptor architecture, however, the truncated PTHR construct used lacked the ~100 residue C-terminal extension harboring the Scribble-interacting PBM motif. Thus, it remains to be clarified if other Scribble regions beyond PDZ1 and three play a role in modulating PTHR signaling.

Because Scribble plays a key role in cell polarity and division, we were concerned as that knockdown in kidney proximal tubules might cause a Fanconi-like syndrome with non-specific electrolyte, solute, and fluid loss. However, the mice are viable and, following knockdown, maintained normal weights and, hence, are not dehydrated. As glucose is entirely absorbed by proximal tubules, non-specific tubular damage would cause glucose loss. Therefore, we measured blood glucose as a control. Targeted loss of Scribble in proximal tubules resulted in pronounced alterations to serum phosphate and vitamin D levels, whereas glucose, calcium, PTH and FGF23 levels remained unaffected. Calcium is generally thought to be the primary regulator of PTH release, with phosphate playing a lesser role. Further, FGF23 suppresses PTH release. Together, this may explain the apparent absence of a change in PTH levels. Further, Scribble knockdown in MDCK cells did not prevent growth to confluence or normal polarization (Fig. 1 *A*–*C*). Together, these findings suggest that, like NHERF1, Scribble modulates PTHR signaling and function in a targeted manner, and reveals a novel and unexpected molecular link between Scribble cell polarity signaling and renal metabolic homeostasis.

GPCRs have emerged as pivotal regulators of metabolic function and energy homeostasis, and their dysregulation manifests in many human diseases (31, 32). Phosphate homeostasis is tightly linked to PTHR activity, with serum phosphorus levels regulated by the interplay of parathyroid hormone, kidney, and bone (33). PTHR activates the 25-hydroxyvitamin D_3-1α-hydroxylase catalyzing the formation of biologically active 1,25$(OH)_2$-vitamin D_3. The present findings support the view that asymmetric PTHR activation is responsible for signaling selectivity and functionality regulating phosphate transport and vitamin D levels. Disordered mineral-ion balance in secondary hyperparathyroidism and chronic kidney disease–mineral and bone disorder (CKD-MBD) may arise from or be ensuant to uncoupled PTHR localization and abundance. It is tempting to speculate that PTHR is bilaterally distributed to apical and basolateral surfaces in polarized proximal nephron cells consequent to NHERF1 and Scribble tethering, respectively. Indeed, our results show that via removal of endogenous Scribble with subsequent reintroduction of exogenous Scribble PTHR localization to the basolateral surface can be manipulated. The distal nephron lacks NHERF1 (34) but expresses Scribble, and here PTHR is associated exclusively with basolateral surfaces.

We conclude that the present findings reveal an adaptor protein axis featuring the PDZ proteins NHERF1 and Scribble that tunes PTHR signaling and localization to legislate and integrate mineral-ion and vitamin D homeostasis.

Materials and Methods

Cell Line. MDCK-shScrib cells, generously shared by Prof. Yasuyuki Fujita (35), express a tetracycline-inducible short hairpin RNA to knock down Scribble expression. We stably transfected HA-tagged PTHR (in pcDNA3.1+) into these cells using Lipofectamine 3,000 (ThermoFisher). HA-PTHR expressing cells were selected using DMEM/F12 10% FBS supplemented with 5 mg/mL Blasticidin (Invitrogen) and 800 μg/mL G418 (Invitrogen), and subcloned using limiting dilution into 96-well plates. Clones from single cells were tested for PTHR expression by immunoblotting protein lysates using a rabbit anti-HA primary antibody (Covance Catalog# PRB-101P) and tested for PTH-stimulated cAMP formation. Scribble knockdown was accomplished by treating cells with 10 μg/mL tetracycline or 30 μg/mL doxycycline overnight.

Plasmid Construct. HA-mCherry-SCRIB was generated using HA-hSCRIB-pcDNA (36). The sequence containing HA-tagged SCRIB was PCR-amplified using the TGACGCTAGCATGTATCCCTATGACGTC forward and TGGGGATCCGAGGGCACAGGG reverse primers. This appended NheI and BamHI restriction sites on the 5′ and 3′ end of the cDNA for HA-SCRIB. This 6-kb PCR product was gel-purified and digested with NheI and BamHI, followed by cloning into NheI/BamHI digested pmCherry-N1 (Clontech). Successful insertion of the HA-SCRIB cassette was confirmed by Sanger sequencing using the CMV forward primer.

Fluorescence Microscopy. We examined PTHR and ß2AR localization by confocal fluorescence microscopy to determine changes in receptor localization in response to Scribble knockdown. Briefly, PTHR-MDCK-shSCRIB cells were grown on collagen-coated coverslips (BD Falcon) for 48 to 7200A0h to establish polarity. The cells were serum starved and treated overnight, as indicated, with 10 μg/mL tetracycline or 30 μg/mL doxycycline, as indicated, to knock down Scribble expression. In cells where rescue of the knockdown of SCRIB and its effect on PTHR localization were examined, tetracycline-treated coverslips were transfected with HA-mCherry-SCRIB, as indicated, Cells were fixed using 4% paraformaldehyde for 10 min, quenched using 100 mM glycine in PBS, and permeabilized using 0.2% Triton X-100 for 15 min at room temperature. The fixed cells were blocked for 1 h at room temperature in 5% goat serum in PBS. The primary antibodies, mouse anti-HA (Covance MMS-101P), goat anti-SCRIB (Santa Cruz sc-11049),

mouse anti-SCRIB (Santa Cruz sc-374139), rabbit anti-PTHR (obtained from Gramsch Laboratories (Schwabhausen, Germany)), and goat anti-ß2-adrenergic receptor (Abcam ab40834), were diluted 1:100 in blocking buffer and applied to the coverslips overnight at 4 °C. Secondary antibodies were incubated for 45 min at room temperature as follows: Alexa Fluor 546-tagged goat antimouse antibody (Invitrogen A-11030) and Alexa Fluor 594-tagged donkey antigoat antibody (Invitrogen A-11058) were diluted 1:1000 in blocking buffer; Alexa Fluor 405-conjugated goat antirabbit antibody (Invitrogen A-31556), Alexa Fluor 488-tagged goat antimouse antibody (Invitrogen A-11001), and Alexa Fluor 488-tagged donkey antigoat antibody (Invitrogen A-11055) were diluted 1:100 in blocking buffer. Coverslips were mounted for immunofluorescence microscopy and analyzed using an Olympus FluoView 1,000 microscope with an ×63 oil immersion objective. Images were processed using Image J (37).

Protein Expression and Purification. Human Scribble PDZ1, 2, 3, and 4 domains were expressed and purified as previously described (23). Scribble PDZ1 and PDZ3 mutants were expressed and purified as previously described (38).

Isothermal titration calorimetry. Purified human Scribble PDZ domains were used in titration experiments against peptides spanning the C-terminus of PTHR to measure their affinity for Scribble PDZ domains. PTHR PBM peptides used were synthesized by Genscript (Uniprot accession number: Q03431) with the following sequences: 4-mer (ETVM), 8-mer (QEEWETVM), and 22-mer (DEEASGPERPPALLQEEWETVM). Titrations were performed at 25 °C with a stirring speed of 750 rpm using the MicroCal(TM) iTC200 System (GE Healthcare) as previously described (39). A protein concentration of 75 μM against a peptide concentration of 900 μM was used. Raw thermograms were processed with MicroCal Origin® version 7.0 software (OriginLabTM Corporation) to obtain the binding parameters of each interaction.

Protein Crystallization, Data Collection, and Refinement. Complexes of PDZ1 with PTHR PBM peptides were reconstituted by mixing protein and peptide at a 1:2 molar ratio as previously described (39). Crystallization trials were performed using 96-well sitting-drop trays (Swissci) and vapor diffusion at 20 °C in-house. 0.15 μL of protein-peptide complexes were mixed with 0.15 μL of various crystallization conditions using a Gryphon nanodispenser robot (Art Robbins). Crystals were obtained at 15 mg/mL in 43% (w/v) polyethylene glycol 300, 0.1 M phosphate-citrate pH 5.2. The PDZ1-PTHR PBM crystals were flash-cooled at 100 K using liquid nitrogen. Rhomboid-shaped crystals were obtained belonging to space group $P4_32_12$. For PDZ3:PTHR PBM, crystals were obtained at 15 mg/mL in 0.1 M Sodium Cacodylate pH 5.8 and 53% MPD. Diffraction data were collected on the MX2 beamline at the Australian Synchrotron using an Eiger 16M detector with an oscillation range of 0.1° per frame using a wavelength of 0.9537 Å, integrated with Xia2 (40) and scaled using AIMLESS (41). The structures were solved by molecular replacement using Phaser (42) with human Scribble PDZ1 [PDB accession code 6MTV (25)] or human Scribble PDZ3 [PDB accession code 5VWI (23)] as search models. The solutions produced by Phaser were manually rebuilt over multiple cycles using Coot (43) and refined using PHENIX (44). Data collection and refinement statistics details are summarized in Table 1. Coordinate files have been deposited in the Protein Data Bank under accession codes 8BIA (PDZ1:PTHR) and 8BJ0 (PDZ3:PTHR). All images were generated using the PyMOL Molecular Graphics System, Version 2.5 Schrödinger, LLC. All raw diffraction images were deposited on the SBGrid Data Bank (45) using their PDB accession codes 8BIA (PDZ1:PTHR) and 8BJ0 (PDZ3:PTHR).

Molecular Dynamics Simulation. The initial coordinates used in MD simulations were taken from the PDB accession codes 8BIA (PDZ1:PTHR) and 8BJ0 (PDZ3:PTHR). All missing hydrogen atoms were added using PyMol (46). The Leap module of AMBER16 with ff99SB force field (47) was used to generate the topology and coordinate files. The model was solvated with TIP3P water molecules in a periodically replicated box with a cutoff of 10 Å, neutralized with sodium ions, and energy minimized over 500 steps, including 100 steps of steepest descent minimization using the pmemd module of AMBER16 (47). Except for the length, the simulation details, equilibration, and production simulations were set according to our previous studies (48, 49). In brief, the water molecules were equilibrated under constant temperature and constant pressure (NPT) conditions at 300 K for 0.8 ns with harmonic restraints applied to the ligand residues and methodically lowered from $k_s = 5.0$ kcal/mol/Å^2 to 0.1 kcal/mol/Å^2. Then, equilibration was performed under constant temperature and constant volume (NVT) at 300 K for 50 ns. The production simulations were carried out for 200 ns at 300 K using the NVT ensemble with an integration step of 2 fs. Weak harmonic restrains ($k_s = 0.1$ kcal/mol/Å^2) were applied to the N-terminal backbone atoms of the PTHR-P 8-mer peptide ligand (-Q^{-7}E^{-6}E^{-5}W^{-4}E^{-3}T^{-2}V^{-1}M^{0}) and PDZ1 or PDZ3 to prevent diffusion from the simulation box. The equilibration phase and the production simulations were monitored by computing the rsmd of the backbone atoms (N, Cα, C) of PDZ1 or PDZ3 and PTHR peptide relative to the initial coordinates. Both complexes achieved equilibration after approximately 50 ns of MD simulation. After that, the RMSD values of PDZ1 or PDZ3 remained relatively low between 2 and 2.5 Å over the entire simulation. The stably fluctuated RMSD values of PTHR peptide between 1 and 1.8 Å suggest that PBM-bound PDZ3 does not change its binding pose in the binding pocket compared to the initial experimentally determined binding mode. In contrast, PTHR peptide-bound PDZ1 is more flexible and fluctuates between 1 and 3 Å.

Mice. We studied the role of Scribble in the polarity of PTHR signaling in proximal tubules by crossing *Scribble*$^{flox/flox}$ mice (50) with *SLC34a1*-GFPCreERT2 (*SLC34a1*$^{GCE/+}$) mice (51). CRE recombinase was expressed exclusively in proximal tubules and was inducible with tamoxifen, enabling tissue-specific knockout of *Scribble*. Mice were genotyped at 28 d by tail biopsy, and a blood sample was taken for glucose and phosphate analysis. Animals that were genotyped as Scribble$^{flox/flox}$ homozygous and SLC34a1-GFPCreERT2 (SLC34a1$^{GCE/+}$) heterozygous were used for all experiments and were also used for breeding. Age and sex matched animals were selected for the corn oil vehicle and tamoxifen treatment groups. Tamoxifen (Sigma-Aldrich) was dissolved in 3% (vol/vol) ethanol containing corn oil (Sigma- Aldrich) at a concentration of 10 mg/mL. At 8 wk of age, 3 mg tamoxifen, or 3% ethanol/corn oil vehicle, was injected intraperitoneally every other day three times on Monday, Wednesday, and Friday. One week after the final injection, mice were anesthetized with isoflurane. Blood was extracted via cardiac puncture in a heparin-treated syringe. Red blood cells were pelleted, and the supernatant was saved for analysis of glucose and phosphate.

We measured glucose and phosphate in samples of blood extracted during genotyping and again with a sample collected at the time of sacrifice. Glucose was analyzed with the Aviva Accu-Chek blood glucose meter using TrueTrack test strips. Plasma phosphate was measured with the Phosphate Colorimetric Kit (Sigma, MAK030). Vitamin D_3 was measured as described (52) on littermate pairs. 1,25 vitamin D_3, 24,25 vitamin D_3, and 25 vitamin D_3 forms were normalized to control levels and combined. PTH and FGF23 were measured with a Luminex 200™ Multiplex Assay (University of Pittsburgh Hillman Cancer Center, Luminex Facility).

Data, Materials, and Software Availability. All study data are included in the article and/or supporting information. Coordinate files have been deposited in the Protein Data Bank under accession codes 8BIA (PDZ1:PTHR) and 8BJ0 (PDZ3:PTHR). All raw diffraction images were deposited on the SBGrid Data Bank (45) using their PDB accession codes 8BIA (PDZ1:PTHR) and 8BJ0 (PDZ3:PTHR).

ACKNOWLEDGMENTS. We thank the staff at the MX beamlines at the Australian Synchrotron for help with X-ray data collection, and the Comprehensive Proteomics Platform at La Trobe University for core instrument support. We are grateful to Dr. L. Banks for contributing HA-hSCRIB-pcDNA. This research was undertaken in part using the MX2 beamline at the Australian Synchrotron, part of Australian Nuclear Science and Technology Organisation, and made use of the Australian Cancer Research Foundation detector. This work was supported in whole or part by the National Health and Medical Research Council Australia (Project Grant APP1103871 to P.O.H. and M.K.; Senior Research Fellowship APP1079133 to P.O.H.) and La Trobe University (Research focus area "Understanding Disease" project grant and scholarships to B.Z.S. and A.J., and by R01 DK111427-01A1 from the NIH to P.A.F. The funders had no involvement in this study.

Author affiliations: [a]Department of Biochemistry & Chemistry, La Trobe Institute for Molecular Science, La Trobe University, Melbourne, VIC 3086, Australia; [b]Laboratory for GPCR Biology, Department of Pharmacology and Chemical Biology, University of Pittsburgh, Pittsburgh, PA 15261; [c]Department of Pharmacy and Therapeutics, Center for Clinical Pharmaceutical Sciences, University of Pittsburgh Schools of Pharmacy and Medicine, Pittsburgh, PA 15216; [d]Department of Medicine Schools of Pharmacy and Medicine Renal-Electrolyte Division, University of Pittsburgh, Pittsburgh, PA 15216; [e]Department of Biochemistry & Pharmacology, University of Melbourne, Melbourne, VIC 3010, Australia; and [f]Department of Clinical Pathology, University of Melbourne, Melbourne, VIC 3010, Australia

1. W. J. Nelson, Adaptation of core mechanisms to generate cell polarity. *Nature* **422**, 766–774 (2003).
2. L. E. Dow, P. O. Humbert, Polarity regulators and the control of epithelial architecture, cell migration, and tumorigenesis. *Int. Rev. Cytol.* **262**, 253–302 (2007).
3. R. Stephens *et al.*, The scribble cell polarity module in the regulation of cell signaling in tissue development and tumorigenesis. *J. Mol. Biol.* **430**, 3585–3612 (2018).
4. T. T. Bonello, M. Peifer, Scribble: A master scaffold in polarity, adhesion, synaptogenesis, and proliferation. *J. Cell Biol.* **218**, 742–756 (2019).
5. D. Bilder, M. Li, N. Perrimon, Cooperative regulation of cell polarity and growth by Drosophila tumor suppressors. *Science* **289**, 113–116 (2000).
6. M. J. Santoni, R. Kashyap, L. Camoin, J. P. Borg, The Scribble family in cancer: Twentieth anniversary. *Oncogene* **39**, 7019–7033 (2020), 10.1038/s41388-020-01478-7.
7. I. Elsum, L. Yates, P. O. Humbert, H. E. Richardson, The Scribble-Dlg-Lgl polarity module in development and cancer: From flies to man. *Essays Biochem.* **53**, 141–168 (2012).
8. Z. Songyang *et al.*, Recognition of unique carboxyl-terminal motifs by distinct PDZ domains. *Science* **275**, 73–77 (1997).
9. V. K. Subbaiah, C. Kranjec, M. Thomas, L. Banks, PDZ domains: The building blocks regulating tumorigenesis. *Biochem. J.* **439**, 195–205 (2011).
10. F. Ye, M. Zhang, Structures and target recognition modes of PDZ domains: Recurring themes and emerging pictures. *Biochem. J.* **455**, 1–14 (2013).
11. S. Hirano, R. Goto, Y. Uchida, SWATH-based comprehensive determination of the localization of apical and basolateral membrane proteins using mouse liver as a model tissue. *Biomedicines* **10**, 383 (2022).
12. M. Kaufmann *et al.*, Apical and basolateral parathyroid hormone receptors in rat renal cortical membranes. *Endocrinology* **134**, 1173–1178 (1994).
13. N. Amizuka *et al.*, Cell-specific expression of the parathyroid hormone (PTH)/PTH-related peptide receptor gene in kidney from kidney-specific and ubiquitous promoters. *Endocrinology* **138**, 469–481 (1997).
14. J. Ba, D. Brown, P. A. Friedman, Calcium-sensing receptor regulation of PTH-inhibitable proximal tubule phosphate transport. *Am. J. Physiol. Renal. Physiol.* **285**, F1233–1243 (2003).
15. J. A. Ardura, B. Wang, S. C. Watkins, J. P. Vilardaga, P. A. Friedman, Dynamic Na+-H+ exchanger regulatory factor-1 association and dissociation regulate parathyroid hormone receptor trafficking at membrane microdomains *J. Biol. Chem.* **286**, 35020–35029 (2011).
16. B. Wang *et al.*, Na/H exchanger regulatory factors control parathyroid hormone receptor signaling by facilitating differential activation of G(alpha) protein subunits. *J. Biol. Chem.* **285**, 26976–26986 (2010).
17. S. J. Reshkin, J. Forgo, H. Murer, Functional asymmetry in phosphate transport and its regulation in opossum kidney cells: Parathyroid hormone inhibition. *Pflugers Arch.* **416**, 624–631 (1990).
18. A. Marchese, M. M. Paing, B. R. Temple, J. Trejo, G protein-coupled receptor sorting to endosomes and lysosomes. *Annu. Rev. Pharmacol. Toxicol.* **48**, 601–629 (2008).
19. C. M. Tan, A. E. Brady, H. H. Nickols, Q. Wang, L. E. Limbird, Membrane trafficking of G protein-coupled receptors. *Annu. Rev. Pharmacol. Toxicol.* **44**, 559–609 (2004).
20. J. Pieczynski, B. Margolis, Protein complexes that control renal epithelial polarity. *Am. J. Physiol. Renal. Physiol.* **300**, F589–601 (2011).
21. D. Bilder, N. Perrimon, Localization of apical epithelial determinants by the basolateral PDZ protein Scribble. *Nature* **403**, 676–680 (2000).
22. J. Y. How, R. K. Stephens, K. Y. B. Lim, P. O. Humbert, M. Kvansakul, Structural basis of the human scribble-vangl2 association in health and disease. *Biochem. J.* **478**, 1321–1332 (2021).
23. K. Y. B. Lim, N. J. Godde, P. O. Humbert, M. Kvansakul, Structural basis for the differential interaction of scribble PDZ domains with the guanine nucleotide exchange factor beta-PIX. *J. Biol. Chem.* **292**, 20425–20436 (2017).
24. K. E. Meier, M. D. Snavely, S. L. Brown, J. H. Brown, P. A. Insel, alpha 1- and beta 2-adrenergic receptor expression in the madin-darby canine kidney epithelial cell line. *J. Cell Biol.* **97**, 405–415 (1983).
25. S. Caria *et al.*, Structural analysis of phosphorylation-associated interactions of human MCC with scribble PDZ domains. *FEBS J.* **286**, 4910–4925 (2019).
26. B. Wang, A. Bisello, Y. Yang, G. G. Romero, P. A. Friedman, NHERF1 regulates parathyroid hormone receptor membrane retention without affecting recycling. *J. Biol. Chem.* **282**, 36214–36222 (2007).
27. M. J. Mahon, M. Donowitz, C. C. Yun, G. V. Segre, Na(+)/H(+) exchanger regulatory factor 2 directs parathyroid hormone 1 receptor signalling. *Nature* **417**, 858–861 (2002).
28. W. B. Sneddon *et al.*, Activation-independent parathyroid hormone receptor internalization is regulated by NHERF1 (EBP50). *J. Biol. Chem.* **278**, 43787–43796 (2003).
29. J. Y. How, S. Caria, P. O. Humbert, M. Kvansakul, Crystal structure of the human scribble PDZ1 domain bound to the PDZ-binding motif of APC. *FEBS Lett.* **593**, 533–542 (2019).
30. L. H. Zhao *et al.*, Structure and dynamics of the active human parathyroid hormone receptor-1. *Science* **364**, 148–153 (2019).
31. I. Tzameli, GPCRs - pivotal players in metabolism. *Trends Endocrinol. Metab.* **27**, 597–599 (2016).
32. L. F. Barella, S. Jain, T. Kimura, S. P. Pydi, Metabolic roles of G protein-coupled receptor signaling in obesity and type 2 diabetes. *FEBS J.* **288**, 2622–2644 (2021).
33. S. J. Khundmiri, R. D. Murray, E. Lederer, PTH and vitamin D. *Compr. Physiol.* **6**, 561–601 (2016).
34. J. B. Wade, P. A. Welling, M. Donowitz, S. Shenolikar, E. J. Weinman, Differential renal distribution of NHERF isoforms and their colocalization with NHE3, ezrin, and ROMK. *Am. J. Physiol. Cell Physiol.* **280**, C192–198 (2001).
35. M. Norman *et al.*, Loss of scribble causes cell competition in mammalian cells. *J. Cell Sci.* **125**, 59–66 (2012).
36. M. Thomas, P. Massimi, C. Navarro, J. P. Borg, L. Banks, The hScrib/Dlg apico-basal control complex is differentially targeted by HPV-16 and HPV-18 E6 proteins. *Oncogene* **24**, 6222–6230 (2005).
37. C. A. Schneider, W. S. Rasband, K. W. Eliceiri, NIH image to imageJ: 25 years of image analysis. *Nat. Methods* **9**, 671–675 (2012).
38. A. Javorsky, P. O. Humbert, M. Kvansakul, Structural basis of the avian influenza NS1 protein interactions with the cell polarity regulator scribble. *Viruses* **14**, 583 (2022).
39. J. C. Maddumage, B. Z. Stewart, P. O. Humbert, M. Kvansakul, Crystallographic studies of PDZ domain-peptide interactions of the scribble polarity module. *Methods Mol. Biol.* **2256**, 125–135 (2021).
40. G. Winter, xia2: An expert system for macromolecular crystallography data reduction. *J. Appl. Crystallogr.* **43**, 186–190 (2010).
41. M. D. Winn *et al.*, Overview of the CCP4 suite and current developments. *Acta Crystallogr. D Biol. Crystallogr.* **67**, 235–242 (2011).
42. L. C. Storoni, A. J. McCoy, R. J. Read, Likelihood-enhanced fast rotation functions. *Acta Crystallogr. D Biol. Crystallogr.* **60**, 432–438 (2004).
43. P. Emsley, K. Cowtan, Coot: Model-building tools for molecular graphics. *Acta Crystallogr. D Biol. Crystallogr.* **60**, 2126–2132 (2004).
44. P. D. Adams *et al.*, PHENIX: A comprehensive python-based system for macromolecular structure solution. *Acta Crystallogr. D. Biol. Crystallogr.* **66**, 213–221 (2010).
45. P. A. Meyer *et al.*, Data publication with the structural biology data grid supports live analysis. *Nat. Commun.* **7**, 10882 (2016).
46. Anonymous, The PyMOL molecular graphics system (Schrödinger, LLC., 2006).
47. D. A. Case *et al.*, *Amber 2023* (University of California, San Francisco, 2023).
48. T. Mamonova, M. Kurnikova, P. A. Friedman, Structural basis for NHERF1 PDZ domain binding. *Biochemistry* **51**, 3110–3120 (2012).
49. T. Mamonova *et al.*, Origins of PDZ binding specificity. A computational and experimental study using NHERF1 and the parathyroid hormone receptor. *Biochemistry* **56**, 2584–2593 (2017).
50. B. Hartleben *et al.*, Role of the polarity protein scribble for podocyte differentiation and maintenance. *PLoS One* **7**, e36705 (2012).
51. T. Kusaba, M. Lalli, R. Kramann, A. Kobayashi, B. D. Humphreys, Differentiated kidney epithelial cells repair injured proximal tubule. *Proc. Natl. Acad. Sci. U.S.A.* **111**, 1527–1532 (2014).
52. J. R. Stubbs, S. Zhang, P. A. Friedman, T. D. Nolin, Decreased conversion of 25-hydroxyvitamin D3 to 24,25-dihydroxyvitamin D3 following cholecalciferol therapy in patients with CKD. *Clin. J. Am. Soc. Nephrol.* **9**, 1965–1973 (2014).